Kassan et al., http://www.jcb.org/cgi/content/full/jcb.201305142/DC1

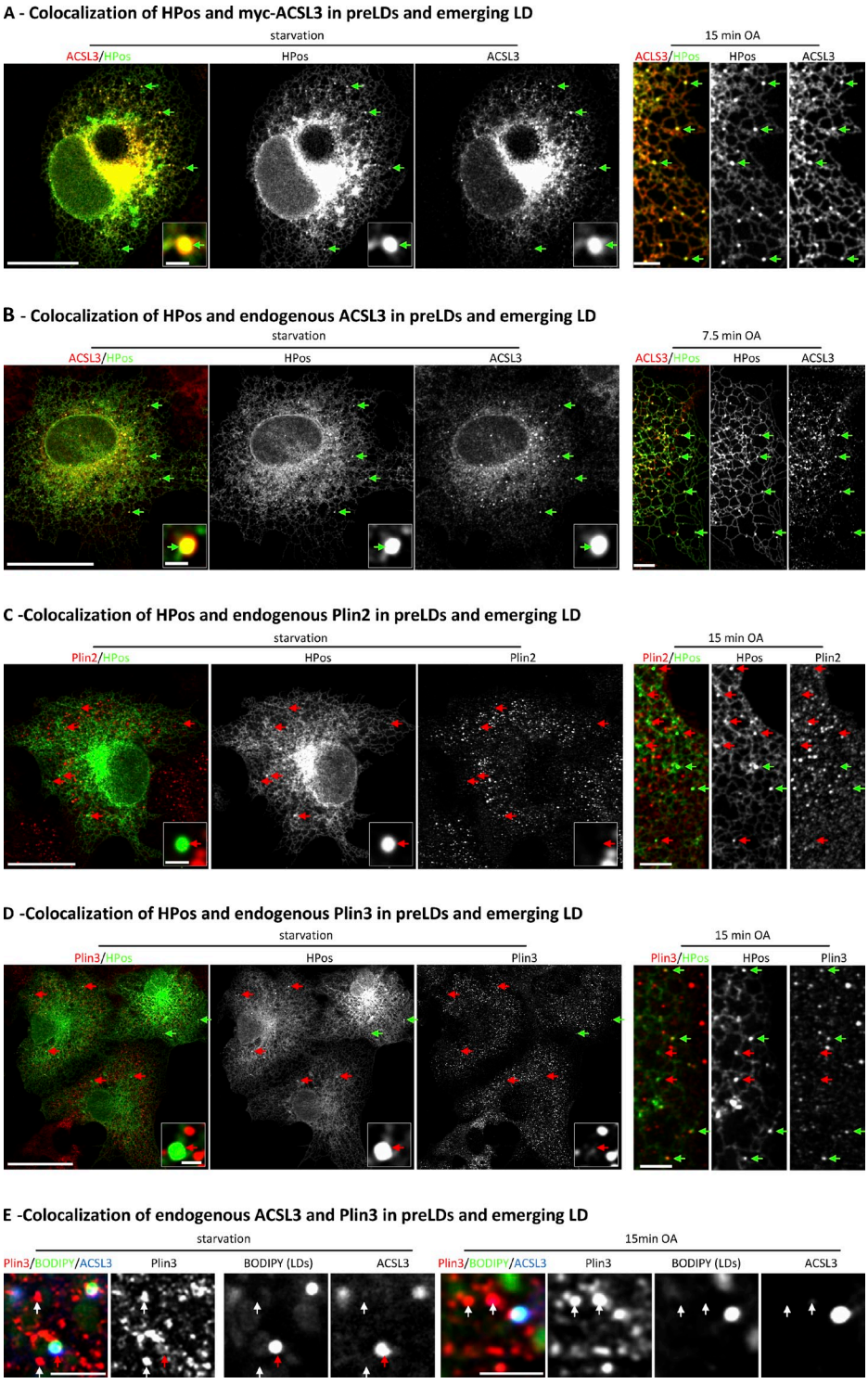

Figure S1. **Detailed colocalization between the proteins analyzed in this study.** This figure is a supplement to Fig. 5. (A) Cells were cotransfected with GFP-HPos and myc-ACSL3 and starved for 24 h (left) or additionally treated with OA for 15 min (right). (B) Endogenous ACSL3 was detected with a specific antibody in starved HPos-transfected cells (left) and in cells additionally treated with OA for 7.5 min (right). The figure shows that the transfected and the endogenous ACSL3 completely colocalized with HPos in pre- and emerging LDs. (C and D) Endogenous Plin2 (red in C) and Plin3 (red in D) were detected with specific antibodies in starved HPos-transfected cells (left) and in cells additionally treated with OA for 15 min (right). Plin2 and Plin3 demonstrate only partial colocalization with HPos; the green arrows indicate colocalization and the red arrows indicate pre-LDs and emerging LDs that are HPos positive but Plin negative. Altogether, these results suggest that ACSL3 is earlier than Plin proteins on emerging LDs. Bars: (left) 25 µm; (insets) 0.5 µm; (right) 5 µm. (E) To test if Plin2 is present in a different subpopulation of LDs that exclude ACSL3, endogenous Plin3 (red) and endogenous ACSL3 (blue) were detected with specific antibodies, and the LDs were labeled with BODIPY 493/503 (green) in starved cells (left) and in cells additionally treated with OA for 15 min (right). White arrows indicate the structures that are positive for Plin3 but negative for ACSL3 and BODIPY and thus that are not LDs. Red arrows indicate again that some LDs contain ACSL3 but not Plin3. Bars, 2 µm.

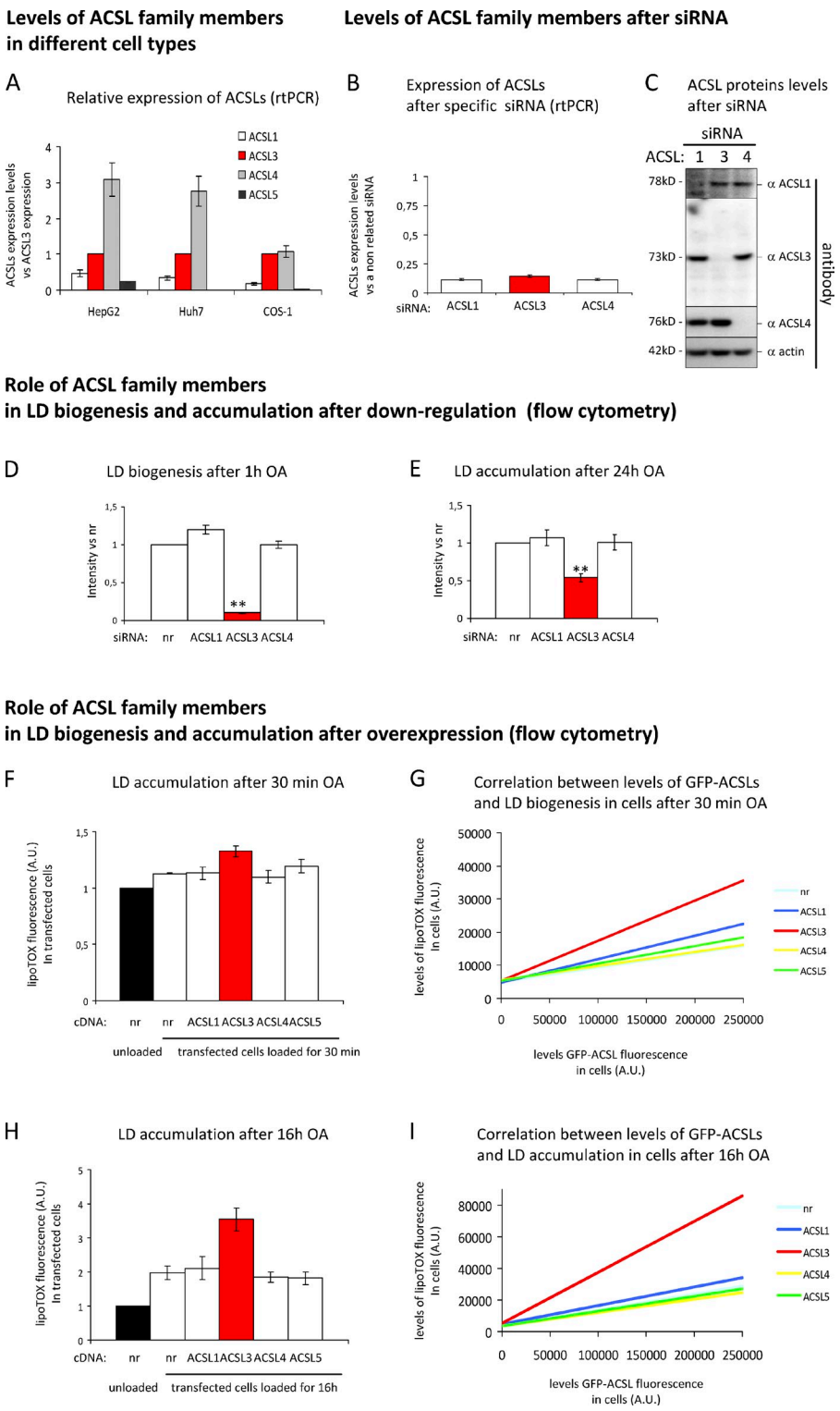

Figure S2. **Role of other ACSL family members in LD assembly and neutral lipid accumulation.** This figure is a supplement to Fig. 7. (A) The relative expression levels of ACSL3 in the cell lines used in this study (see hepatic cells in Fig. S4) was compared with the expression of other ACSL family members by qRT-PCR (the value of ACSL3 in each cell line was normalized to 1). (B and C) COS-1 cells were transfected for 24 h with the siRNA corresponding to ACSL1, ACSL3, or ACSL4 and then additionally starved for 24 h. The percentage of RNA expression levels of each isoform at this time point, with respect to a nonrelated siRNA (nr), was determined by real-time PCR (B), and the specificity of each siRNA for the corresponding family member confirmed by Western blotting of cell homogenates (C). (D and E) Next, neutral lipids were quantified with Nile red and flow cytometry in the siRNA-transfected cells after the starvation period and after an additional treatment with OA for 1 h (D) or 24 h (E). **, $P < 0.01$. (F–I) To demonstrate that only ACSL3 determines LD levels, even when the ACSL enzymes are expressed to identical levels, COS-1 cells were transfected with the indicated GFP-tagged ACSL isoforms or with the GFP and starved for 24 h. Cells were then treated with OA for 30 min (F and G) or 16 h (H and I). LDs were labeled using LipidTOX Deep red, and the transfected cells were identified in the flow cytometer by the presence of green fluorescence. The graphs in F and H show the mean intensity of LDs (red fluorescence) in transfected cells (GFP positive), quantified in three independent experiments and normalized to the red fluorescence of unloaded GFP-transfected cells. The graphs in G and I show a representative trend line of the red fluorescence (LD levels) quantified in cells with increasing levels of expression of each GFP-ACSL (green fluorescence intensity). Altogether, these results demonstrate that ACSL3 is the family member that determines biogenesis and accumulation of LDs in COS-1 cells. Error bars indicate the standard deviation of at least three independent experiments.

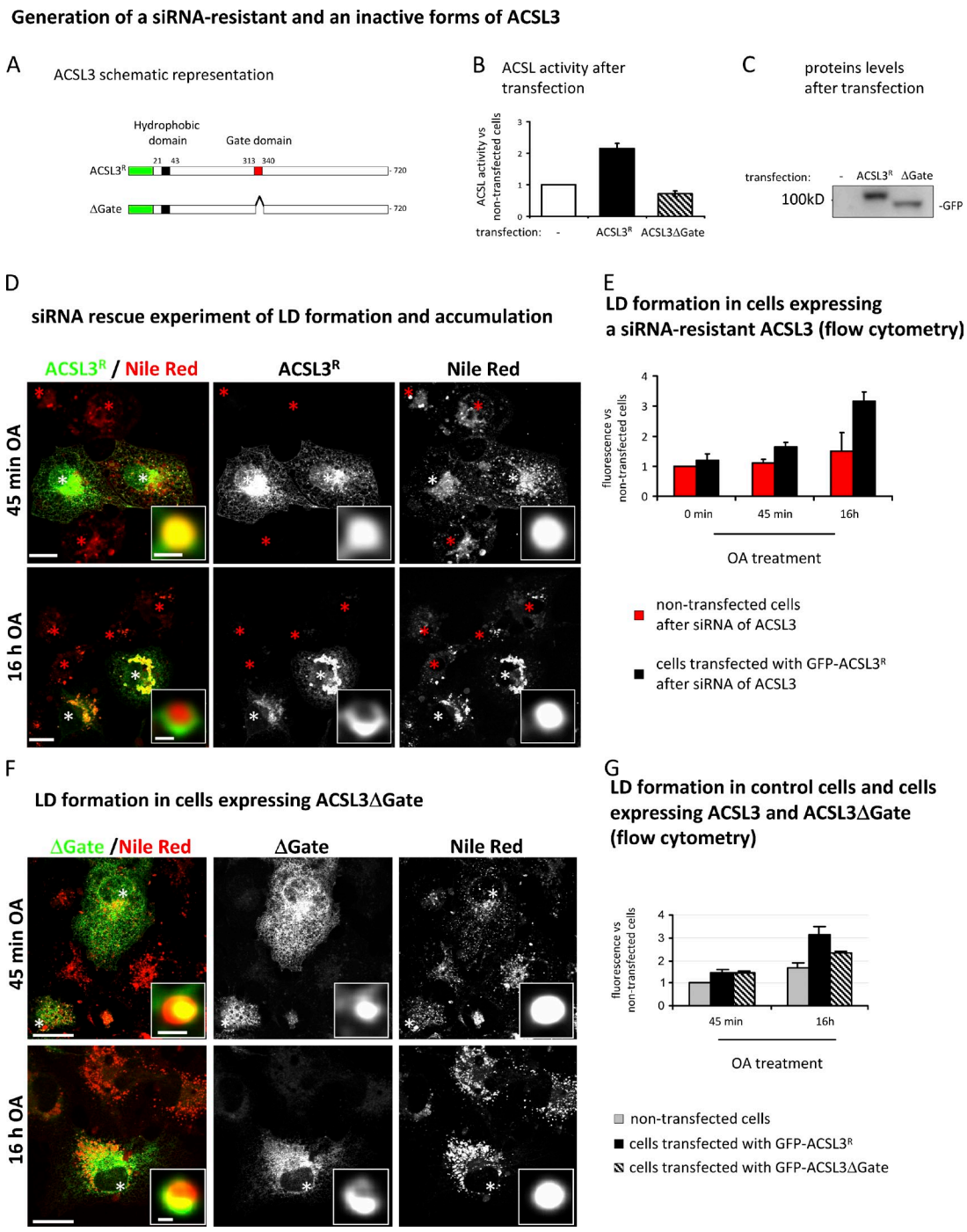

Figure S3. **siRNA rescue experiment and the likely scaffolding role of ACSL3 during LD biogenesis.** This figure is a supplement to Fig. 7. (A) Schematic representation of the proteins used in the figure; an siRNA-resistant form of ACSL3 (ACSL3^R) and an inactive form of ACSL3 generated by deletion of the residues corresponding to the Gate domain (ACSL3ΔGate). Although no conclusive structural information is available for the mammalian acyl-CoA synthetases (Soupene and Kuypers, 2008), in the specific case of ACSL6, the fatty acid Gate domain motif is essential for the activity of the human isoform (Soupene et al., 2010). Because this region is conserved in mammalian ACSLs, we generated a GFP-tagged ACSL3 without the Gate domain (red letters in Fig. S5 B). (B and C) The acyl-CoA synthetase activity was quantified in control COS-1 cells and in cells additionally transfected with ACSL3^R or ACSL3ΔGate. In contrast to the full-length GFP-ACSL3, the GFP-ACSL3ΔGate did not demonstrate detectable enzymatic activity (B), although the expression of both proteins was similar when analyzed by Western blotting of cell homogenates with anti-GFP antibodies (C). (D and E) To rule out off-target effects of the siRNAs used in this study, starved ACSL3-depleted cells, by means of the siRNA, were transfected for 24 h with ACSL3^R and then incubated for 45 min or 16 h with OA. Neutral lipids were labeled with Nile red and analyzed by confocal microscopy (D) or with LipidTOX and flow cytometry (E). The expression of ACSL3^R rescued the inhibition caused by the siRNA of ACSL3 in the assembly and accumulation of LDs. The insets show representative emerging and mature LDs, and the asterisks indicate the transfected cells. (F and G) Finally, starved ACSL3ΔGate-transfected cells were also incubated for 45 min or 16 h with OA, and neutral lipids were stained with Nile red and analyzed by microscopy (F) or with LipidTOX and flow cytometry (G). After 45 min, the ACSL3ΔGate-transfected cells demonstrated an increased accumulation of LDs when compared with cells transfected with GFP, which was similar to the increment caused by the full-length GFP-tagged ACSL3. The ACSL3ΔGate-expressing cells also demonstrated a relative increase in neutral lipid accumulation when treated with OA for 16 h. This lends support to the hypothesis that not only the enzymatic activity of ACSL3 but also other properties of the enzyme cooperate during LD nucleation, and that the activity of the enzyme is involved in LD growth and expansion (see Discussion). The GFP-ACSL3ΔGate showed a preferential accumulation in one side of the LDs (high-magnification insets in F), which suggests that the fatty acid Gate domain partially determines the transport of the enzyme into LDs. White asterisks indicate transfected cells. Bars: (main panels) 25 µm; (insets) 2 µm. Error bars indicate the standard deviation of at least three independent experiments.

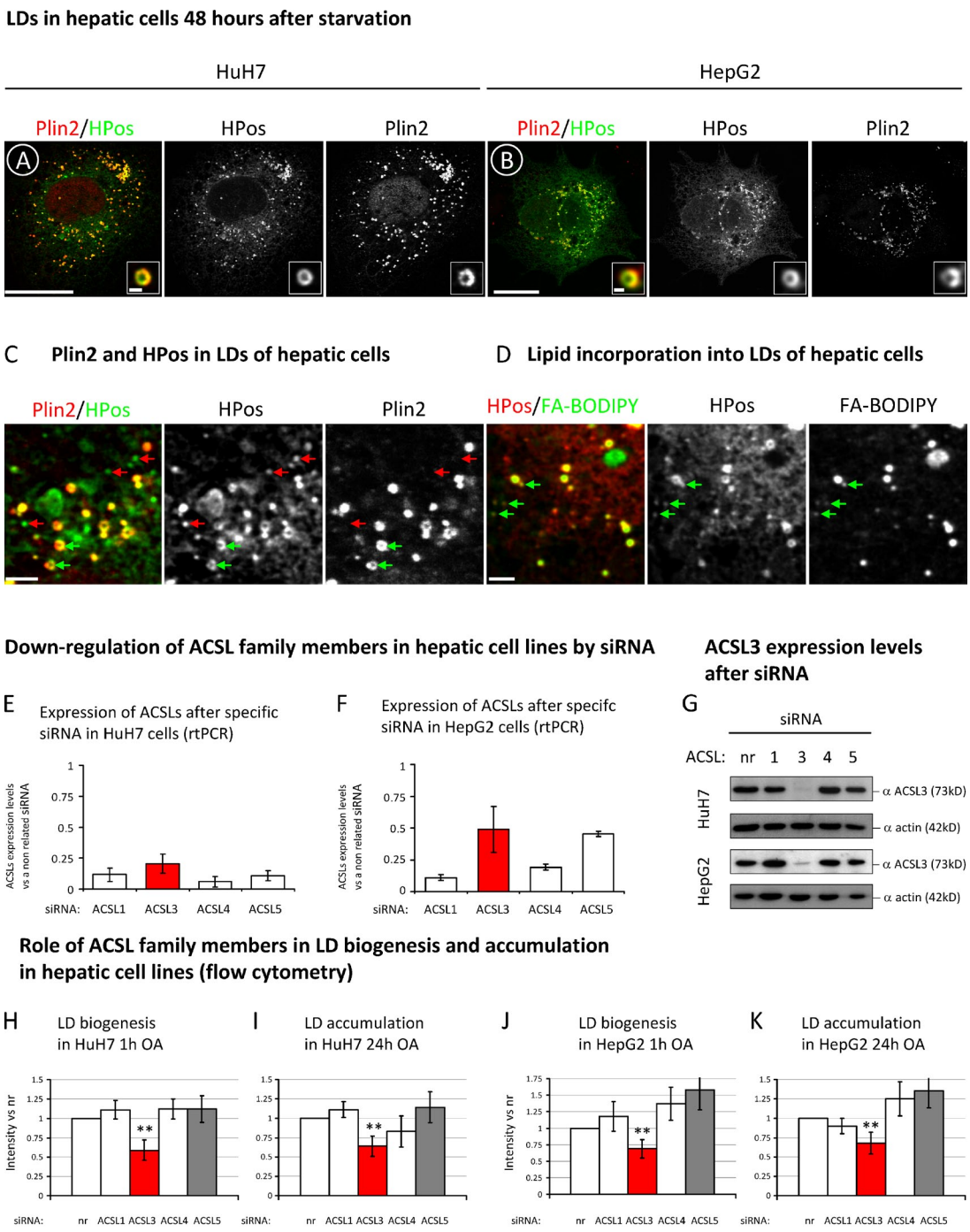

Figure S4. **ACSL3 regulates LD assembly and neutral lipid accumulation in hepatic cell lines.** This figure is a supplement to Fig. 7. To analyze the role of ACSL3 during LD formation and accumulation in other cell lines, we tested the effect of the ACSLs siRNA in human hepatic cell lines, such as HuH7 and HepG2. (A–C) First, GFP-HPos–transfected HuH7 (A and C) and HepG2 (B) cells were starved for 48 h. Distributions of HPos (green) and endogenous Plin2 (red) were analyzed by confocal microscopy. The images show that the starvation conditions that efficiently removed LDs in COS-1 cells did not completely eliminate the presence of LDs in hepatic cells even when prolonged for 48 h. In contrast to the pre-LDs of COS-1 cells, the number of LDs observed in hepatic cells after starvation was partially reduced by Triacsin C or Platensimycin, a specific inhibitor of the fatty acid synthase (not depicted), which suggests that during starvation these LDs are supplied with newly synthesized fatty acids. After 48 h of starvation, HPos formed a characteristic ring around mature LDs that colocalized with endogenous Plin2 (A, B, and green arrows in C). The red arrows indicate HPos-positive but Plin2-negative structures. Thus, several structures positive for HPos and negative for Plin2, which could be equivalent to the pre-LDs observed in COS-1 cells, are also present in hepatic cells (C, red arrows). The insets show a representative mature LD. Bars: (A and B) 25 µm; (insets) 0.5 µm; (C) 2 µm. (D) To analyze lipid packaging in these cells, OFP-HPos–transfected HuH7 cells were treated as in Fig. 4 with the FA-BODIPY for 15 min. Cells were fixed, and lipid distribution was analyzed by microscopy. The green arrows indicate that the FA-BODIPY was rapidly packed in the small HPos-positive LDs and in the mature LDs. Bar, 2 µm. (E–K) To study the role of ACSL3 during lipid packaging, HuH7 and HepG2 cells were transfected for 24 h with the siRNAs corresponding to ACSL1, ACSL3, ACSL4, or ACSL5 and then additionally starved for 24 h. The RNA levels after each siRNA were measured by real-time PCR (A and B) and shown in the graph as a percentage with respect to cells transfected with a nonrelated siRNA (nr). The ACSL3 protein levels were additionally analyzed by Western blotting of cell homogenates (G). The cells were then loaded for 1 h or 24 h with OA, neutral lipids were stained with Nile red, and cellular fluorescence was quantified by flow cytometry. Only when ACSL3, but not other family members, was down-regulated were the early accumulation of neutral lipids and the long-term accumulation of LDs significantly reduced, which suggests that ACSL3 is the family member that regulates LD formation and accumulation in hepatic cell lines. Error bars indicate the standard deviation of at least three independent experiments. **, $P < 0.01$.

A

Amino acid sequence and *in silico* analysis of alpha-helix formation by the positive sequence of HPos

```
1  lfeaigkifsniristqkei
```

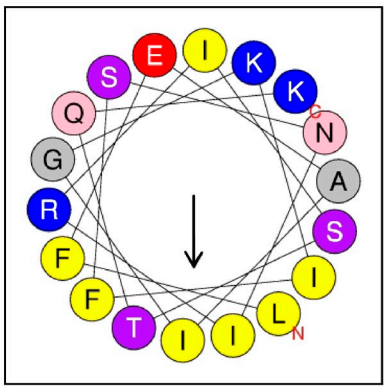

B

Amino acid sequence and examples of *in silico* analysis of alpha-helix formation by human ACSL3

```
  1 mnnhvsskps tmklkhtinp illyfihfli slytiltyip fyffsesrqe ksnrikakpv
 61 nskpdsayrs vnsldglasv lypgcdtldk vftyaknkfk nkrllgtrev lneedevqpn
121 gkifkkvilg qynwlsyedv fvrafnfgng lqmlgqkpkt niaifcetra ewmiaaqacf
181 mynfqlvtly atlggpaivh alnetevtni itskellqtk lkdivslvpr lrhiitvdgk
241 pptwsefpkg iivhtmaave algakasmen qphskplpsd iavimytsgs tglpkgvmis
301 hsniiagitg maeripelge edvyigylpl ahvlelsael vclshgcrig ysspqtladq
361 sskikkgskg dtsmlkptlm aavpeimdri yknvmnkvse mssfqrnlfi laynykmeqi
421 skgrntplcd sfvfrkvrsl lggnirlllc ggaplsattq rfmnicfccp vgqgygltes
481 agagtisevw dyntgrvgap lvcceiklkn weeggyfntd kphprgeili ggqsvtmgyy
541 kneaktkadf fedengqrwl ctgdigefep dgclkiidrk kdlvklqage yvslgkveaa
601 lknlplvdni cayansyhsy vigfvvpnqk eltelarkkg lkgtweelcn scemenevlk
661 vlseaaisas lekfeipvki rlspepwtpe tglvtdafkl krkelkthyq adiermygrk
```

AAISASLEKFEIPVKIRL[142]

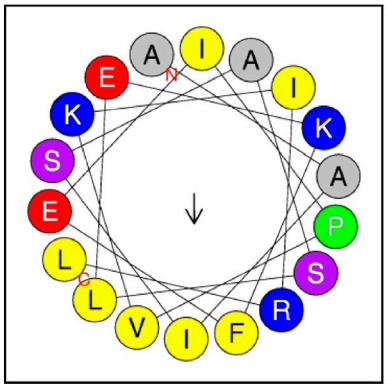

GTWEELCNSCEMENEVLK[120]

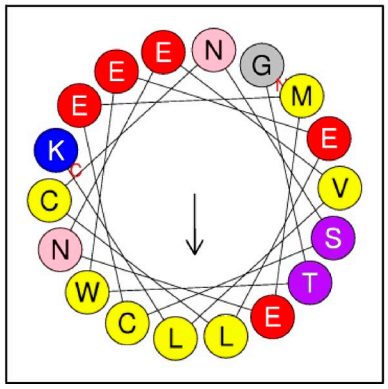

VIGFVVPNQKELTELARK[98]

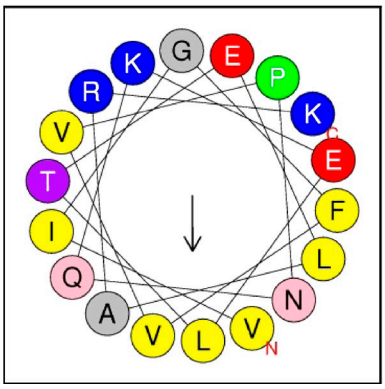

Figure S5. **Putative amphipathic α helices in HPos and ACSL3.** This figure is a supplement to the Discussion section. The figure shows the amino acid sequence and the in silico analysis of putative amphipathic α helices predicted by the HELIQUEST program (http://heliquest.ipmc.cnrs.fr/) to be formed by HPos and the human form of ACSL3 (three representative sequences; Gautier et al., 2008). In each helix, the hydrophobic amino acids (yellow) are enriched on the opposite side to negative (red) and positive (blue) residues.

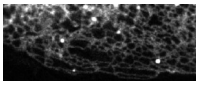

Video 1. **Starved GFP-HPos–transfected COS-1 cells were treated with cycloheximide for 30 min.** This video corresponds to Fig. 3 A. Images were analyzed by time-lapse confocal microscopy using a laser scanning confocal spectral microscope (TCS SP5; Leica) equipped with an incubation control system (37°C, 5% CO_2). Cells were selected for the labeling of well-defined tubular ER elements. In starved cells, pre-LDs were followed for 5 min (images were captured every 1.3 s). Next, OA (175 µg/ml) was added (indicated with OA in left bottom corner) and images were captured for an additional 15 min every 9 s.

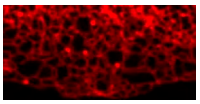

Video 2. **Images of starved COS-1 cells transfected with orange-HPos (red) were analyzed by time-lapse confocal microscopy using a laser scanning confocal spectral microscope (TCS SP5; Leica) equipped with an incubation control system (37°C, 5% CO_2).** This video corresponds to Fig. 2 A (merged channels). Cells were selected for the labeling of well-defined tubular ER elements. In starved cells, pre-LDs were followed for 5 min (images were captured every 1.3 s). Cells were then loaded with OA (175 µg/ml) that additionally contained a BODIPY-tagged fatty acid (1 µM, green). Images were captured for an additional 15 min every 9 s.

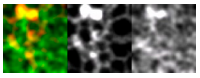

Video 3. **The three channels (merge channels, red for HPos, and green for FA-BODIPY) of two selected pre-LDs and one emerging LD shown in Video 2.** This video corresponds to Fig. 2 A (separated channels). As in Video 2, starved COS-1 cells transfected with orange-HPos (red) were analyzed using a laser-scanning confocal spectral microscope (TCS SP5; Leica). Cells were selected for the labeling of well-defined tubular ER elements. In starved cells, pre-LDs were followed for 5 min (images were captured every 1.3 s). Cells were then loaded with OA (175 µg/ml) that additionally contained a BODIPY-tagged fatty acid (1 µM, green). Images were captured for an additional 15 min every 9 s.

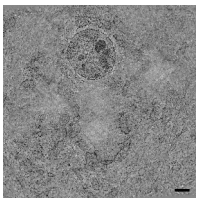

Video 4. **Starved COS-1 cells were treated for 10 min with OA and then submitted to a second starvation for an additional 16 h.** This video corresponds to Fig. 9. Cells were processed with no primary fixative and a very quick nonperturbing freeze substitution protocol. 300-nm HM20 sections, nonspecifically labeled with gold as fiducial markers, were tilted ±60° in both axes, taking images every 1 or 2° using an intermediate-voltage EM (Tecnai F30; FEI Company). Bars, 250 nm.

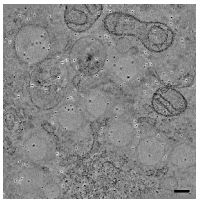

Video 5. **Starved COS-1 cells were treated for 10 min with OA and then submitted to a second starvation for an additional 16 h.** This video corresponds to Fig. 9. Cells were processed with no primary fixative and a very quick nonperturbing freeze substitution protocol. 300-nm HM20 sections, nonspecifically labeled with gold as fiducial markers, were tilted ±60° in both axes taking images every 1 or 2° using an intermediate voltage EM (Tecnai F30; FEI Company). Bars, 250 nm.

References

Gautier, R., D. Douguet, B. Antonny, and G. Drin. 2008. HELIQUEST: a web server to screen sequences with specific alpha-helical properties. *Bioinformatics*. 24:2101–2102. http://dx.doi.org/10.1093/bioinformatics/btn392

Soupene, E., and F.A. Kuypers. 2008. Mammalian long-chain acyl-CoA synthetases. *Exp. Biol. Med. (Maywood)*. 233:507–521. http://dx.doi.org/10.3181/0710-MR-287

Soupene, E., N.P. Dinh, M. Siliakus, and F.A. Kuypers. 2010. Activity of the acyl-CoA synthetase ACSL6 isoforms: role of the fatty acid Gate-domains. *BMC Biochem.* 11:18. http://dx.doi.org/10.1186/1471-2091-11-18